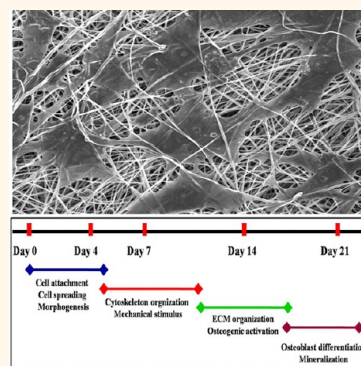


# Lower Extent but Similar Rhythm of Osteogenic Behavior in hBMSCs Cultured on Nanofibrous Scaffolds *versus* Induced with Osteogenic Supplement

Wentao Liu,<sup>†,‡,#</sup> Yan Wei,<sup>†,||,#</sup> Xuehui Zhang,<sup>§,||</sup> Mingming Xu,<sup>†,||</sup> Xiaoping Yang,<sup>†</sup> and Xuliang Deng<sup>†,||,\*</sup>

<sup>†</sup>Department of Geriatric Dentistry, Peking University School and Hospital of Stomatology, Beijing 100081, People's Republic of China, <sup>‡</sup>Key Laboratory of Zoonosis, Ministry of Education, College of Veterinary Medicine, Jilin University, Changchun 130062, People's Republic of China, <sup>§</sup>Department of Materials Science and Engineering, Tsinghua University, Beijing 100084, People's Republic of China, <sup>†</sup>Key Laboratory of Carbon Fiber and Functional Polymers, Ministry of Education, Beijing University of Chemical Technology, Beijing 100029, People's Republic of China, and <sup>||</sup>National Engineering Laboratory for Digital and Material Technology of Stomatology, Beijing 100081, People's Republic of China. <sup>#</sup>W. Liu and Y. Wei contributed equally to this work.

**ABSTRACT** Nanotopographic cues from biomaterials exert powerful effects on the osteogenic differentiation of mesenchymal stem cells because of their niche-mimicking features. However, the biological mechanisms underlying cell lineage determination by surface nanotopography have not been clearly elucidated. Here, we explored the osteogenic behavior of human bone marrow mesenchymal stem cells (hBMSCs) on poly-L-lactide nanofibers with different orientations and monitored the dynamic changes in global gene expression triggered by topographical cues. RT-PCR analysis of osteogenic marker genes and ALP activity assays demonstrated that hBMSCs cultured on random nanofibers showed enhanced osteogenic-specific fate compared with those on aligned nanofibers. Microarray analysis demonstrated a similar temporal change in gene expression patterns between hBMSCs cultured on random nanofibers and those induced with an osteogenic supplement (OS). However, the extent of osteogenic differentiation on the fibrous scaffold was much lower than that driven by chemical OS. In-depth pathway analysis revealed that focal adhesion kinase, TGF- $\beta$ , Wnt, and MAPK pathways were involved in the activation of osteogenic differentiation in hBMSCs on random nanofibers. These findings suggested that a lower extent but similar rhythm of dynamic cellular behavior was induced on random nanofibers when compared with the OS condition and that mechanotransduction could trigger nonspecific and multilevel responses in hBMSCs. This study provides insight into the regulation of osteogenesis directed by substratum surfaces.



**KEYWORDS:** bone tissue engineering · mesenchymal stem cells · nanofibers · osteogenic differentiation · global gene expression

Cell–biomaterial interactions have been shown to exert a considerable influence on the function and differentiation of mesenchymal stem cells (MSCs).<sup>1–4</sup> Recent studies of the effects of nanotopographic cues from biomaterials on the spontaneous osteogenic differentiation of MSCs have shown their powerful role in regulating the osteogenic behavior of stem cells.<sup>5,6</sup> Nanometric-scale shallow pits,<sup>7</sup> grooves,<sup>8</sup> and raised islands<sup>9</sup> have been found to increase the expression of osteoblastic marker proteins and promote the differentiation of MSCs to osteoblasts.<sup>10,11</sup>

Nanofibers, universally accepted as niche-biomimetic scaffolds in bone regeneration, have also been found to enhance the

proliferation and osteogenic differentiation of MSCs.<sup>12,13</sup> Hu *et al.* have reported that MSCs cultured on poly-L-lactide (PLLA) nanofibers exhibit an enhanced osteogenic differentiation phenotype involving higher bone sialoprotein (BSP) and osteocalcin expression and increased alkaline phosphatase (ALP) activity.<sup>14</sup> Yin *et al.* have reported that randomly oriented nanofibers induce higher ALP activities and more calcium deposition, which is related to integrin- and myosin-mediated mechanotransduction.<sup>15</sup> Similar results have been reported in our previous study showing that ALP activity and the production of collagen type I and osteocalcin were all increased in MG63 cells cultured on random PLLA nanofibers.<sup>16</sup>

\* Address correspondence to kqdengxuliang@bjmu.edu.cn.

Received for review April 28, 2013 and accepted August 1, 2013.

Published online August 01, 2013 10.1021/nn402118s

© 2013 American Chemical Society

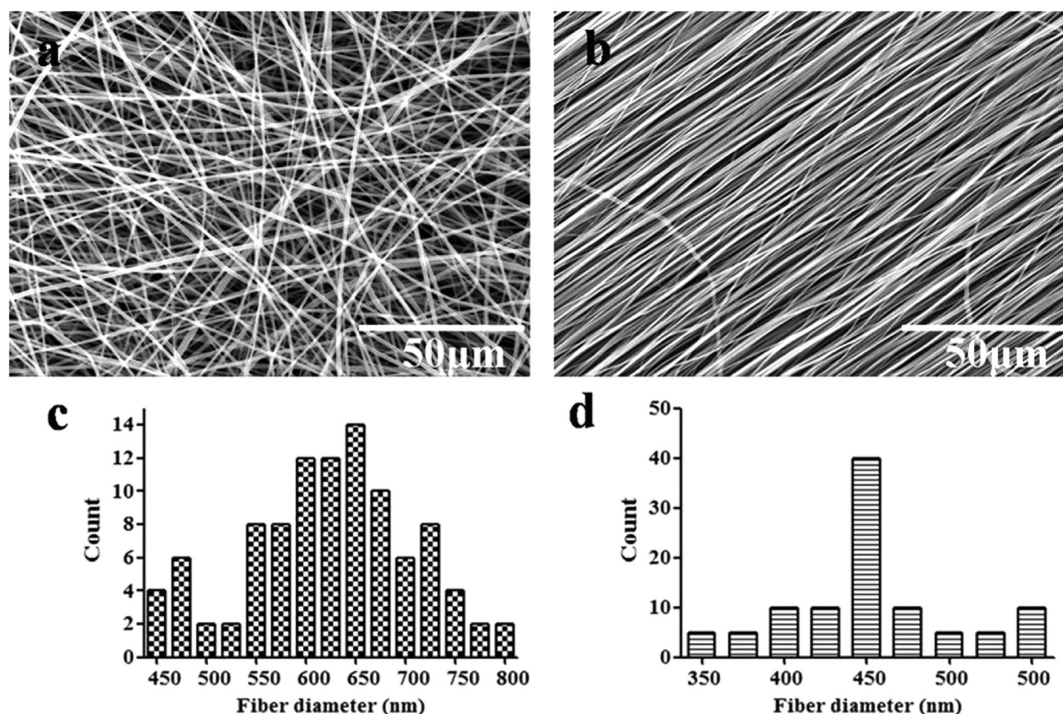


Figure 1. SEM images of PLLA nanofiber scaffolds: (a) random and (b) aligned. The diameters measured of (c) random and (d) aligned nanofibers (nm).

It has been reported that PHBHHx electrospun nanofibers effectively enhance the osteogenic differentiation of MSCs by regulating the MAPK-dependent PPAR signaling pathway.<sup>17</sup> Lim *et al.* found that the nanofiber topography itself is sufficient to mediate stem cell differentiation by promoting the activation of the Wnt signaling pathway.<sup>18</sup> These observations demonstrate that the nanotopographic features of synthetic fibers mimic the extracellular matrix (ECM) and may provide essential niches to guide MSCs' osteogenic behavior.

However, although many reports have described the phenotypic and genotypic phenomena that occur during the nanofibrous scaffold-mediated osteogenic differentiation of MSCs, the biological mechanisms underlying the osteogenic behavior of MSCs in response to nanotopography have not been clearly elucidated.

In this study, temporal changes in the osteogenic behavior and dynamic global gene expression patterns of human bone marrow mesenchymal stem cells (hBMSCs) were assessed during their culture on random and aligned electrospun PLLA nanofibers without an osteogenic supplement (OS). The slow degradation of PLLA might help to preserve the topographic features and eliminate the possible action of chemical cues in this laboratory model. hBMSCs cultured on flat polymer films and induced with OS were used as the positive control. Osteogenic differentiation was examined by real-time quantitative PCR (RT-qPCR) and microarray analysis at 4, 7, 14, and 21 days of culture. In-depth pathway analysis was employed to explore

the possible mechanism triggered by nanotopographic cues. This study provides new insights into the regulation of osteogenesis directed by substratum surfaces, thus extending our ability to control biomaterial–cell interactions and develop novel biomaterials.

## RESULTS

**Characterization of PLLA Nanofibers.** Before cell seeding, 100 fibers of random and aligned PLLA nanofibers were selected to measure their diameters based on the SEM images. As shown in Figure 1, the diameter of random nanofibers was  $624.0 \pm 83.93$  nm, and the diameter of aligned nanofibers was  $450 \pm 50$  nm.

**Morphological Observation of BMSCs on Nanofibers.** After 1 day of culture, hBMSCs on random nanofibers exhibited a highly branched morphology with round nuclei, and those on aligned nanofibers displayed a polarized morphology with oval nuclei along the fiber directions (Figure 2a–f). Furthermore, on random nanofibers, it could be seen that some filament-like structures extend out from the MSC's body and penetrated into the superficial layer of the nanofibrous scaffold. Meanwhile, fewer cell processes of MSCs penetrate into the interstitial space between the aligned nanofibers.

**ALP Activity of BMSCs.** As shown in Figure 3, ALP activity of hBMSCs increased slightly without significance from day 2 to day 4 on random and aligned nanofibers. At day 7, the ALP activity on random nanofibers was 2.0 mU/mL, which was significantly higher than that in culture on aligned nanofibers (1.3 mU/mL) and flat polymer films without OS (1.4 mU/mL). Cells

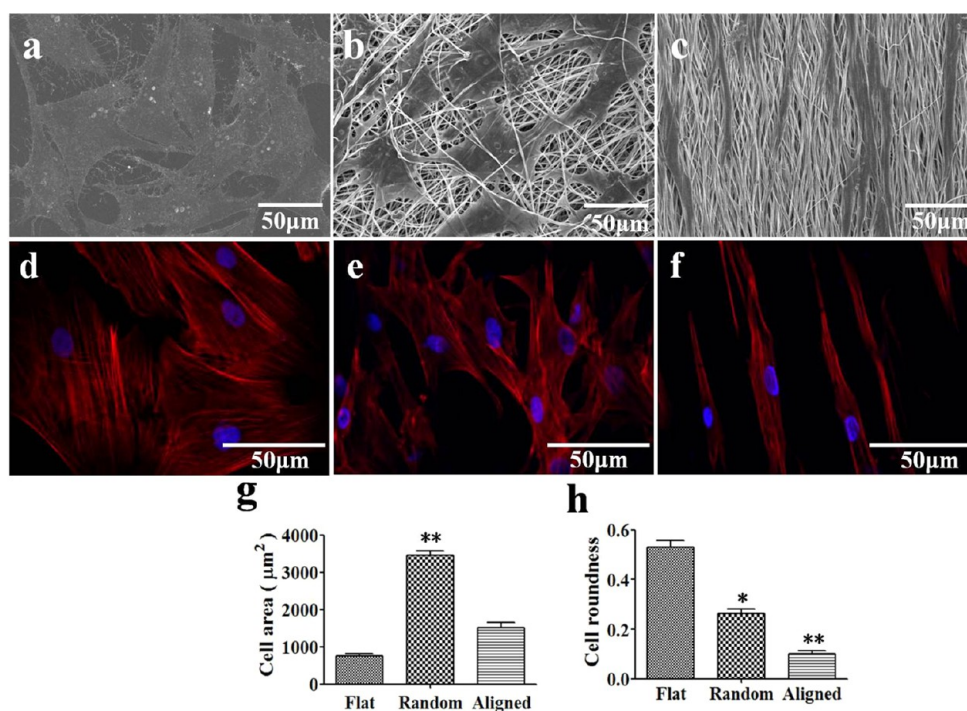


Figure 2. SEM images of hBMSCs after 1 day of culture on (a) flat polymer films, (b) random nanofibers, and (c) aligned nanofibers. Immunofluorescence staining of cytoskeletal actin in hBMSCs on (d) flat polymer films, (e) random nanofibers, and (f) aligned nanofibers (scale bar: 100 μm). Actin is red and nuclei are blue. Cell area (g) and roundness (h) of hBMSCs cultured on flat polymer films and nanofibers. \* $p < 0.05$  and \*\* $p < 0.01$ .

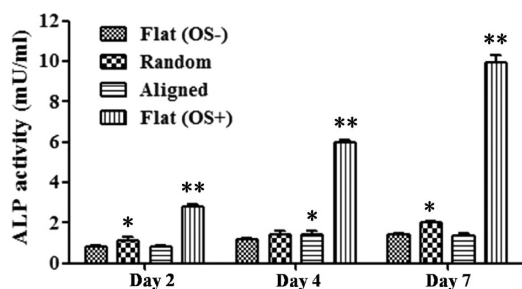


Figure 3. ALP activity in culture supernatants from hBMSCs at days 2, 4, and 7. Error bars are SD ( $n = 3$ ). \* $p < 0.05$  and \*\* $p < 0.01$  ( $n = 3$ ).

cultured on flat polymer films with OS as the positive control showed the highest ALP activity at 2, 4, and 7 days.

**Expression of Osteogenic Marker Genes.** The expression of osteogenic marker genes is shown in Figure 4. hBMSCs cultured on flat polymer films showed nearly unaltered marker gene expression at all time points, whereas they displayed time-dependent dynamic gene expression changes on random nanofibers. BMP2 was steadily up-regulated, reaching a 2.5-fold increase at day 21. RUNX2 was up-regulated (1.5-fold) at day 4, and this up-regulated level was maintained at all other time points. SPP1 and COL1A1 were up-regulated by more than 2-fold at day 4, which was maintained at days 7 and 14, and achieved 5- and 6-fold increases, respectively, at day 21. SPARC was up-regulated by 1.5-fold at days 4 and 7 and by 2-fold at

day 21. The expression level of BSP was steadily up-regulated during culture and achieved a 2-fold increase at day 21, similar to BMP2. Minor changes in these selected osteogenic genes were observed in hBMSCs cultured on aligned nanofibers, which were in the range of  $1.0 \pm 0.3$ -fold. hBMSCs cultured in medium with OS displayed the highest up-regulated expression levels of these selected osteogenic genes at all experiment time points. Interestingly, the same trend of sequential changes in the expression of all selected genes was observed in the random nanofibers group and the OS group.

**Temporal Global Gene Expression Profiles Determined by Microarray Analysis.** Microarray analysis using a GeneChip Human Genome U133 Plus 2.0 was performed on cells at 4, 7, 14, and 21 days. The data discussed in this study have been deposited in the NCBI Gene Expression Omnibus Web site, and the series number is GSE48616. Based on the 47,000 transcripts analyzed, a log–log scatter plot of gene expression significantly influenced by different topographic cues is shown in Figure 5. It shows that the number of up-regulated genes in hBMSCs cultured on random PLLA nanofibers increased from day 4 to 7, then decreased to a relatively lower level at day 14, and finally increased to the highest level at day 21. This trend was similar to that in the OS group. In the aligned group, the number of up-regulated genes increased from day 4 to 7, then decreased from day 7 to 14, and decreased further on day 21. In terms of the number of down-regulated

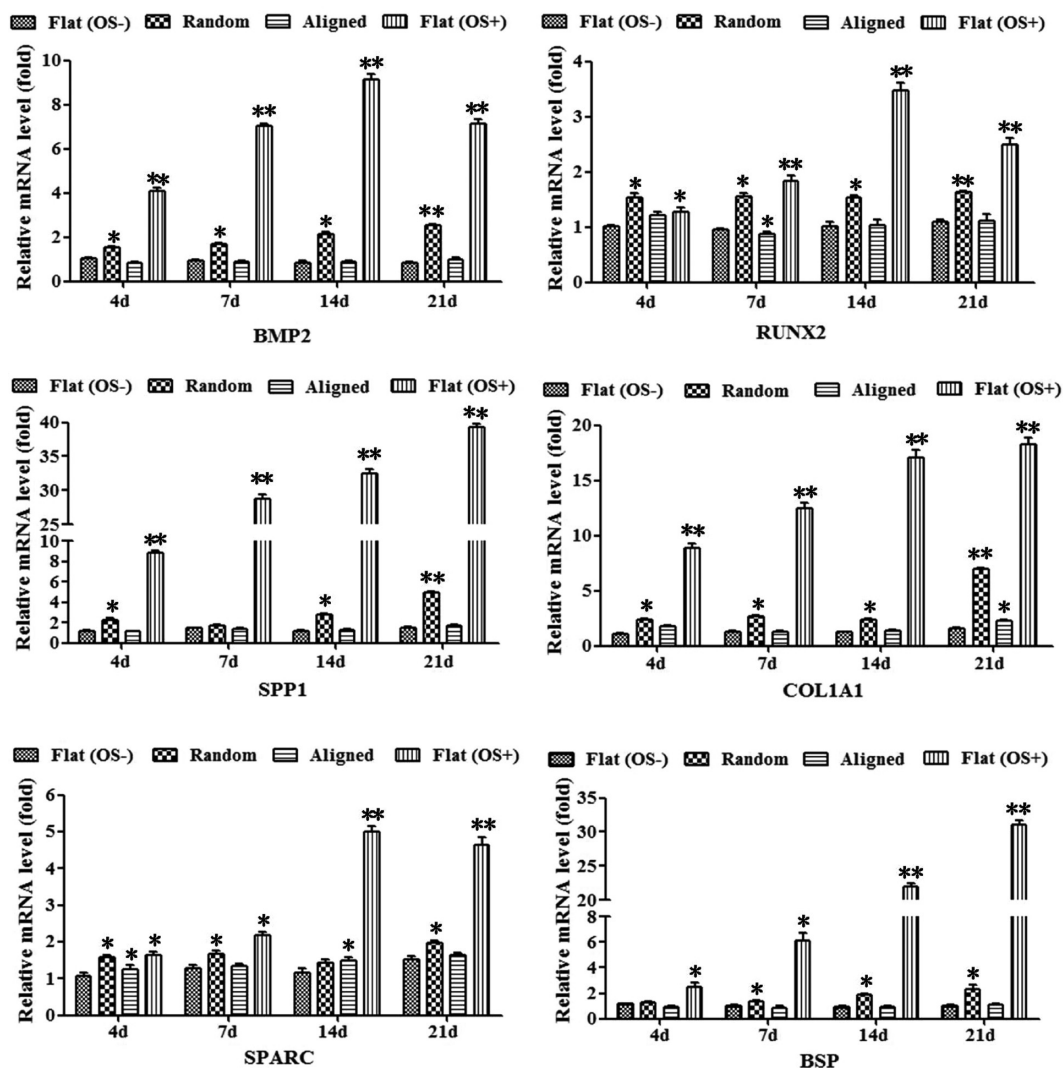


Figure 4. RT-qPCR analysis of gene expression in cells seeded on random and aligned nanofibers and flat polymer films with or without OS. Error bars are SD ( $n = 3$ ). \* $p < 0.05$  and \*\* $p < 0.01$ .

genes, all groups showed a similar trend. To testify the microarray data analysis, mRNA levels of BMP2, RUNX2, SPP1, COL1A1, SPARC, and BSP were validated by RT-qPCR analysis. The results displayed that similar expression patterns of these selected genes were obtained from both RT-qPCR and microarray analysis.

**Gene Ontology.** Temporal patterns of activated genes in hBMSCs in the random and aligned nanofiber groups and under the OS condition are shown in Figure 6. In the random group, genes involved in cell adhesion, ECM organization, and integrin-mediated signaling pathways were up-regulated at day 4. Then, at day 7, expression of genes associated with cytoskeletal organization was observed to increase significantly. At day 14, osteogenic pathways, including TGF- $\beta$ /BMP, MAPK, and Wnt, were up-regulated. At the end of the experiment on day 21, genes associated with mineralization were up-regulated. hBMSCs cultured with OS showed a closely similar dynamic but a much higher magnitude of gene expression changes compared with hBMSCs

cultured on random nanofibers. The changes in gene expression associated with osteogenic differentiation in the aligned nanofibers group in particular were negligible compared with the flat polymer film control. The aligned PLLA fibers appeared to have minimal influence on the osteogenic differentiation of BMSCs.

**Pathway Analysis of Osteogenic Differentiation Induced by Nanofibrous Topographic Cues.** The differentially expressed genes of signaling pathways influenced by random nanofibers are listed in Table 1. A total of 57 genes involved in focal adhesion and morphology were affected. Forty-three genes of the MAPK signaling pathway, 27 genes of the TGF- $\beta$ /BMP signaling pathway, and 22 genes of the Wnt signaling pathway were significantly affected by nanofibers with random orientations. The corresponding molecules in these pathways were further checked by cluster analysis (Figure 7). The results demonstrated that these molecules were responsible for the activation of osteogenic differentiation in hBMSCs.

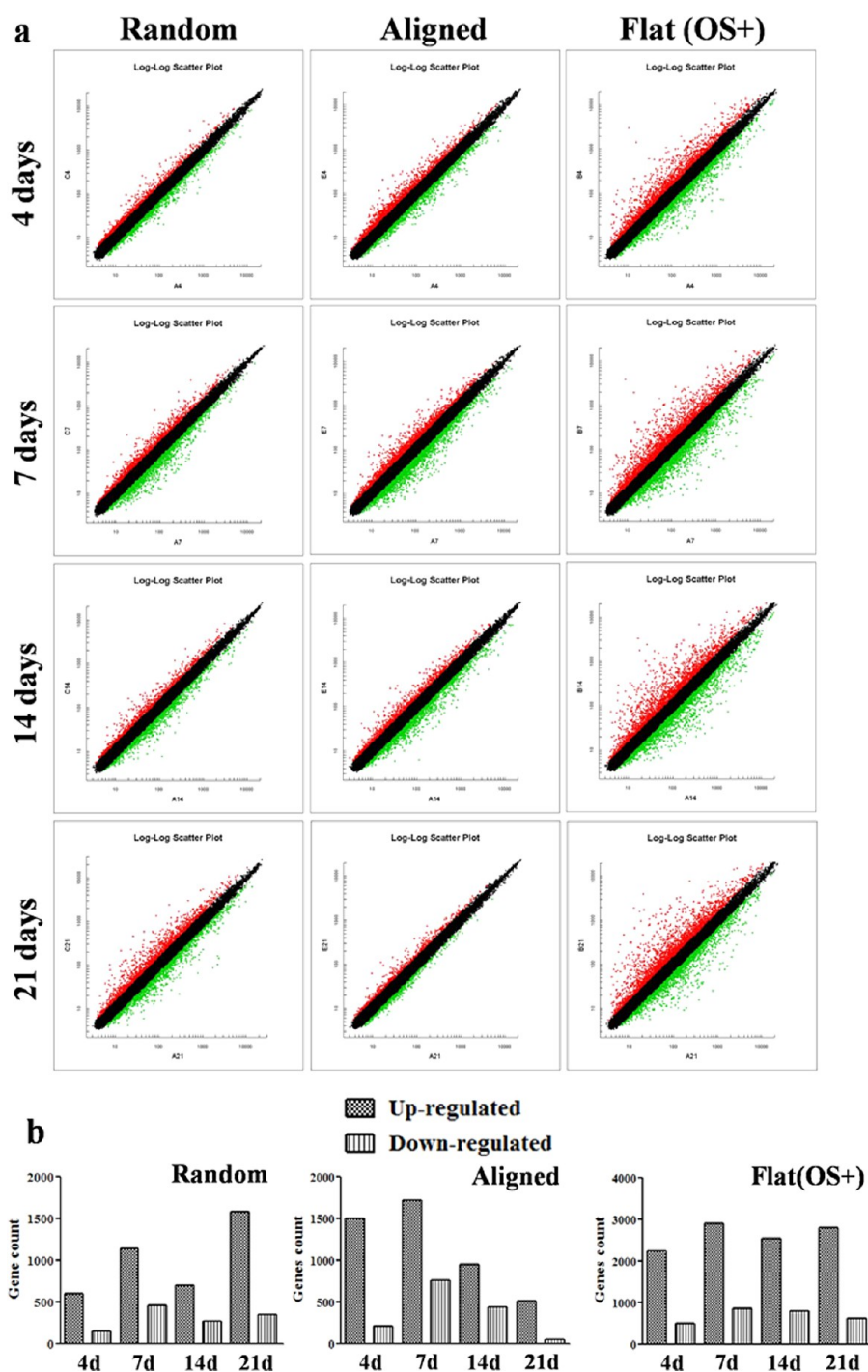


**Figure 5.** Schematic representation of the global gene expression profiles of hBMSCs at 4, 7, 14, and 21 days (a). Red dots represent up-regulated genes, green dots represent down-regulated genes, and black dots represent no difference. The total number of differential gene expression in hBMSCs cultured on nanofibers and on films induced with OS (b). OS caused the most significant influence on genome, followed by the random group and then the aligned group.

## DISCUSSION

Topography has been demonstrated to play important roles in modulating osteogenic tissue development.<sup>19,20</sup> Many reports have shown that the beneficial topographical cues of biomaterials promote the osteogenic functions of stem cells.<sup>21,22</sup> On the basis of the well-established literature, electrospun random nanofibers have been reported to provide actual

osteogenic niches in various aspects. According to the report of Pashuck *et al.*, electrospun random nanofibers could mimic the structure of ECM-derived scaffolds,<sup>23</sup> and their dimension seems to simulate the structure of woven bone, which is the initial bone phenotype formed in the healing process after fracture.<sup>24</sup> In our work, the diameters of the random PLLA fibers mimic those of collagen fibrils in ECM.<sup>25</sup>

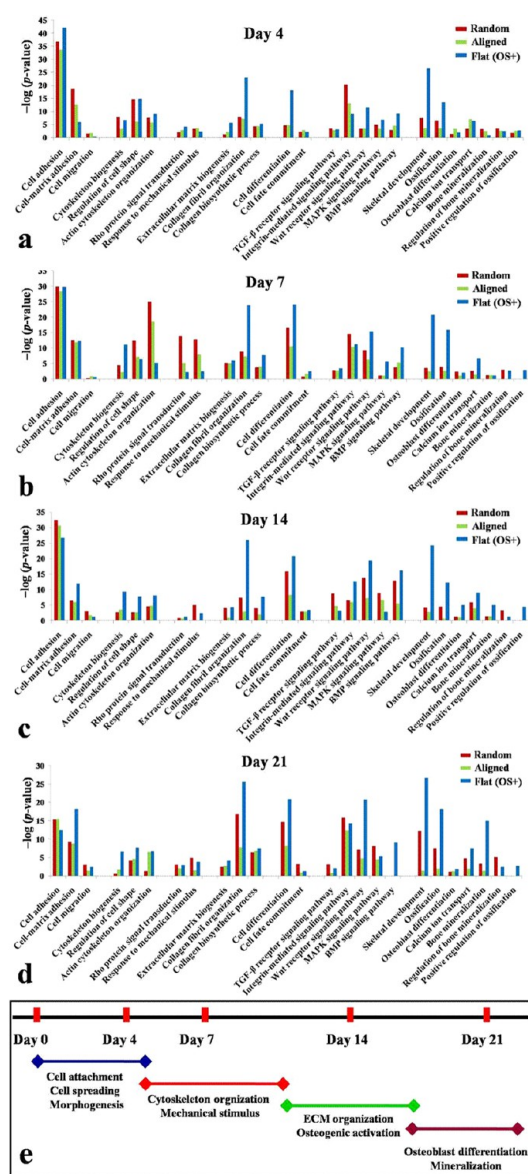


**Figure 6.** Gene ontology analysis of hBMSCs at (a) 4, (b) 7, (c) 14, and (d) 21 days. (e) Graphical summary of the four phases of osteogenic differentiation of hBMSCs triggered by random nanofibers.

The apparent porosity of random PLLA fibers was considered to favor efficient mass transportation of nutrients, oxygen, and waste products.<sup>26</sup> In our previous study, random PLLA nanofibers were found capable of modulating cell morphology through fiber orientation, favoring osteogenic differentiation of BMSCs.<sup>16</sup> This study was performed to monitor the temporal behavior and gene expression dynamics of hBMSCs on PLLA nanofibers.

The morphological changes of hBMSCs on different topographic PLLA nanofibers in this study were consistent with our previous work. These morphological phenotypes of hBMSCs can be explained by the classical theory of contact guidance.<sup>27,28</sup> Cross-lapped and relatively isotropic random nanofibers may favor the

growth of hBMSCs with a highly branched morphology, whereas aligned nanofibers result in an anisotropic mechanical distribution that restricts hBMSCs to the edges and to extend along the fibers. Cytoskeletal reorganization accompanies cell shape changes and leads to spherical nuclei on random fibers and elongated oval nuclei on aligned fibers.<sup>16,29</sup> Cell morphology is considered to be closely correlated with the differentiation state of stem cells, and a branched morphology has been reported to be compatible with osteogenic differentiation.<sup>30,31</sup>

Our results from RT-PCR analysis corroborated the theory of “cellular shape-dependent functions”. Kumar *et al.* considered that a highly branched cell shape can act as an “osteocyte-like” morphology to push hBMSCs toward an osteogenic lineage in the absence of OS.<sup>30</sup> A cellular biomechanical response was considered to be associated with focal adhesions (FA). It has been reported that the small and immature FA of MSCs on aligned nanofibers was considered to represent the cell status of migrating, while the large and supermature FA of MSCs on random nanofibers indicated the cell status of sensing the mechanical properties to act on cell lineage.<sup>17</sup> The gene ontology data presented in this work show high expression of integrins, cell adhesion molecules, and extracellular matrix receptors, which are considered to serve as “outside-in” mechanical sensors and play an important role in regulating cytoskeletal organization.<sup>32–35</sup> Higher expressions of integrins  $\alpha 4$ ,  $\alpha 5$ ,  $\alpha 8$ ,  $\alpha 10$ ,  $\alpha 11$ ,  $\beta 1$ , and  $\beta 3$  in BMSCs cultured on random nanofibers compared to those cultured on aligned ones were found, which suggested that nanotopographical influence on cell behavior could be initiated by the regulation of integrin clustering and the subsequent focal adhesion assembly. Notably upregulated FAK in turn could influence F-actin organization and cell mechanical properties to mediate downstream mechanotransductive effects.<sup>32,36,37</sup> The expression of genes associated with cytoskeletal organization and mechanical stimulation in the random group was significantly up-regulated, while hBMSCs cultured with OS showed lower expression of genes associated with mechanical stimulation and Rho protein signal transduction at all time points. These results supported the theory that mechanotransduction was responsible for the osteogenic differentiation of hBMSCs triggered by random nanofibers.<sup>38</sup> Tseng *et al.* have also demonstrated that intracellular mechanical stresses, including cytoskeletal tension, are able to induce the spontaneous osteogenic differentiation of MSCs.<sup>39</sup> Moreover, it is also well known that high tension and cell spreading are essential for the osteogenic differentiation of MSCs.<sup>2,40</sup>

In our study, the activated state of hBMSCs toward osteogenic differentiation on random PLLA nanofibers was much lower when compared with hBMSCs cultured in OS conditions. Similarly, Tsimbouri *et al.*

TABLE 1. KEGG Signaling Pathways Associated with Osteogenic Genes in Cells Cultured on Random Nanofibers<sup>a</sup>

pathway title	count	genes up-regulated	genes down-regulated
focal adhesion	57	CAN2, COL11A1, ITGA3, DOCK1, VEGFA, COL1A2, COL3A1, ITGAV, FAK, COND2, MYLK, HGF, PAK1, BIRC3, VCL, PDGFRD, PDGFRA, ITGB3, COL5A2, ITGA11, ITGA2, SPP1, COL4A1, COL1A1, COL6A2, ROCK2, PDGFA, LAMA3, THBS2, SHC4, COL5A3, RHOA, JUN, LAMB3, COL4A4, COMP, PLA2G4A, RPS6KA5, CD14, CACNB2, RELB, MAP4K4, PAK1, NTRK2, HSPB1, PDGFRA, FGFR2, RASGRP2, FAS, MAP3K5, MAPKAPK3, GADD45B, TGFBR1, PDGFA, CDC25B, JUN, NTF3, DUSP5, JUN, FGF1	ITGA9, LAMA2, IBSP, IGF1R, ITGA, COL1A26, HGF, TNC, PRKCA, LAMC2, ITGA7, FN1, THBS1, PIK3R3, VEGFB, PDGFA, LAMA4, ITGB8, MET, RAC2, COL6A1
MAPK signaling pathway	43	PLA2G4A, RPS6KA5, CD14, CACNB2, RELB, MAP4K4, PAK1, NTRK2, HSPB1, PDGFRA, FGFR2, RASGRP2, FAS, MAP3K5, MAPKAPK3, GADD45B, TGFBR1, PDGFA, CDC25B, JUN, NTF3, DUSP5, JUN, FGF1	HSPA2, DUSP6, FOS, ACVR1C, STK4, RRSAS2, PRKCA, FGF5, FGF11, FGF7, CACNA1G, GADD45B, TGFB2, DUSP4, DUSP10, RPS6KA2, MAP3K1, RAC2, BDNF
TGF- $\beta$ /BMP signaling pathway	27	ID3, BMP2, ID4, CDKN2B, SMAD9, FST, ACVRL1, ACVR2A, LTBP1, SMAD5, PITX2, ROCK2, TGFBR1, DCN, THBS2, BMP4, COMP, SMAD1, SMAD8	ACVR1C, SMURF2, INHBB, THBS1, BMP6, TGFBR2, NOG, ID1
Wnt signaling pathway	22	CCND2, FZD4, TCF7L2, PRICKLE1, LEFT, FZD8, SFRP1, WNT5, ROCK2, TCF7, WNT3, JUN, FZD5, PLCB4	FOSL1, SFRP2, DAAM2, PRKCA, PORCN, FZD7, NMD2, 4, RAC2

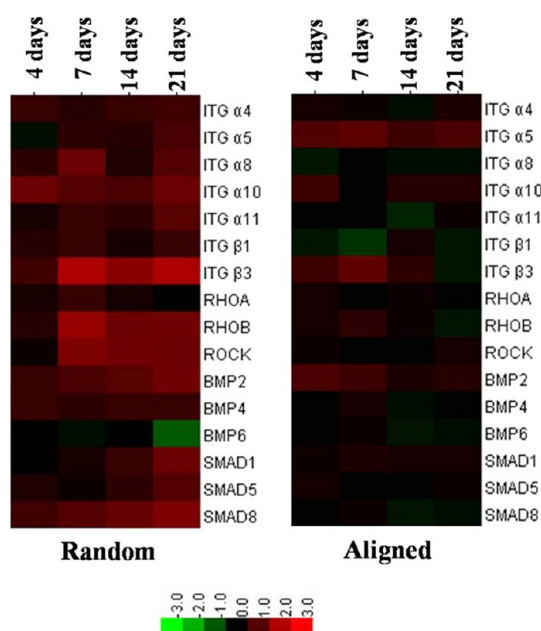
<sup>a</sup> Threshold:  $p$ -value <0.05.

Figure 7. Expression profile of several crucial proteins in osteogenic differentiation pathways. Red and green indicate up- and down-regulation, respectively.

reported that biochemical stimulation is more sensitive and forceful compared with direct or indirect mechanical control in regulating cell fate.<sup>41</sup> They also demonstrated that small RNAs that regulate signaling pathways may be more important in MSC self-renewal and differentiation than the mechanical effect.<sup>42</sup> Although the mechanical stimulations provided by specific nanotopographies are temperate compared with biochemically active factors, they might be necessary for creating and maintaining the niche-mimicking ECM microenvironment and supporting cell differentiation in regenerative medicine to some extent. When MSCs on a niche-mimicking extracellular matrix are induced in an osteogenic medium, the effects would be amplified because of the direct role of the microenvironment in facilitating the osteogenic behavior of stem cells. Kaur *et al.* reported that osteo-specific genes, including osteocalcin, osteopontin, and osteonectin, were up-regulated and showed a maximum enhancement on a nanotopological substratum compared with tissue culture plastic (TCP).<sup>43</sup> PLLA nanofibrous scaffolds were reported to offer a significant supporting role in regulating the osteogenic capacity of hMSCs.<sup>14,30,44</sup> Hence, it can be postulated that the role of the niche-mimicking microenvironment is indispensable in regulating cellular behaviors.

Microarray, gene ontology, and RT-PCR analyses confirmed that the temporal effects of random fibers on BMSCs were similar to those caused by OS. It was found that random fibers share great similarity in the rhythm of osteogenic behavior with that induced by OS. The theory of resonant amplification used in physics might be employed here to explain the synergistic

action of nanotopography and OS on the osteogenic differentiation of hBMSCs. It could be hypothesized here that resonant amplification of the common rhythms of osteogenic behavior of BMSCs on random nanofibers and in the OS condition might account for the amplification of osteogenic differentiation.

In-depth pathway analysis showed activation of FAKs, TGF- $\beta$ /BMP, Wnt, and tension-specific MAPK signaling pathways in highly branched hBMSCs on random fibers. All of these pathways are possibly activated by mechanical stimuli.<sup>36,38</sup> Our results confirmed the finding that topography exerts mechanotransductive effects on cells and plays critical roles in regulating the ECM-induced osteogenic differentiation of MSCs.<sup>45,46</sup> These observations imply that a network of signaling pathways rather than a single signaling pathway is responsible for regulating mechanotransduction-induced osteogenic commitment of hBMSCs. Differences exist in the context of osteogenic differentiation in OS-conditioned medium from that triggered by nanotopography. The components of OS are included to activate specific pathways.<sup>43,47</sup> These

phenomena also suggest that mechanotransduction plays nonspecific and multilevel functions in the osteogenic differentiation of BMSCs.

## CONCLUSION

In this study, the temporal effects of PLLA nanofibers on the cellular behavior and gene expression patterns of hBMSCs were investigated. The ability of hBMSCs to differentiate toward osteogenic lineages on random nanofibers was greater than that on aligned nanofibers. The effects of random nanofibers on lineage determination in hBMSCs might be mediated by mechanotransduction. The rhythm of dynamic changes in osteogenic marker genes and global gene expression patterns was similar to that driven by chemical OS. Topographic cues and chemical OS may exert synergistic effects that enhance the osteogenic differentiation of hBMSCs. A network of pathways consisting of FAK, TGF- $\beta$ , Wnt signaling, and MAPK was involved in the osteogenic differentiation of hBMSCs on PLLA nanofibers, suggesting that mechanotransductive effects might be responsible for nonspecific and multi-level activation of osteogenic differentiation in hBMSCs.

## METHODS

**Fabrication of Electrospun PLLA Nanofiber.** PLLA powder (0.7 g) was added to 10 mL of trifluoroethanol and stirred overnight. The solution was ejected from a 20 mL syringe with a steel needle (inner diameter: 0.5 mm) using a programmable syringe pump (Top 5300, Japan) at a rate of 0.7 mL/h. Using high-voltage equipment (DW-P303--1AC, China) to provide an unremittng voltage (15 kV) to the tip of the needle when a fluid was ejected, a metal plate (20  $\times$  25 cm<sup>2</sup>) was used as a collector at a distance of 18 cm from the tip of the needle to obtain randomly arranged PLLA nanofibers. A cylindrical drum, which rotated at a surface linear rate of 12 m/s, was used as a collector to obtain aligned PLLA nanofibers. To fabricate flat PLLA films, the PLLA polymer solution was casted on a flat glass plate and dried at 50  $^{\circ}$ C for 3 h. All these samples (PLLA nanofibers and flat films) were kept in a vacuum oven (DZF-6210, Bluepard, China) at room temperature for 2 weeks to remove residual solvent. The fiber diameters ( $n = 100$ ) were measured from SEM images using image analysis software (Image J; National Institutes of Health, USA).

**Cell Culture and Seeding on PLLA Nanofibers.** The hBMSCs used in this research were supplied by Cyagen Biosciences Inc., and they were obtained as surgical waste material from normal male donors aged 20–30 years old. The culture medium was human mesenchymal stem cell basal medium containing 10% mesenchymal stem cell-qualified fetal bovine serum, 10  $\mu$ g/mL glutamine, and 100 IU/mL penicillin–streptomycin (all purchased from Cyagen Biosciences Inc.). The medium was changed every 2–3 days. At 80–90% confluence, hBMSCs were detached with 0.25% trypsin/EDTA (Gibco) and subcultured at a density of  $5 \times 10^5$  cells per T75 flask. Third passage hBMSCs were used in this study. PLLA nanofiber scaffolds and flat polymer films were cut into 2.5  $\times$  2.5 cm<sup>2</sup> pieces and fixed between the cap and the centrifugal tubes (50 mL) as in our previous work.<sup>16</sup> After placed into six-well plates, these devices were sterilized with ultraviolet light for 1 h, immersed in 70% ethanol for 10 min, and then washed three times with phosphate-buffered saline (PBS). Cells cultured on flat polymer films in medium with OS comprising 50 mg/mL ascorbic acid, 10 mM sodium b-glycerol phosphate, and  $10^{-8}$  M dexamethasone were used as positive controls. Negative controls were cells

cultured on flat polymer films without any osteogenic additives. The hBMSCs were seeded on each sample in the same manner at a density of  $5.0 \times 10^4$  cells.

**Morphological Observation and Fluorescence Staining of Cytoskeletal Actin.** Cell morphology was observed by SEM with an accelerating voltage of 15 kV. At 1 day after cell seeding, hBMSCs cultured on nanofibers were washed with PBS, fixed with 2.5% glutaraldehyde, and then treated with 0.18 M sucrose. After three rinses with water, the samples were dehydrated through a series of graded alcohol solutions and then air-dried overnight. Prior to observation, the cells were coated with gold using a Jeol JFC-1200 fine coater. For fluorescence staining, cells were fixed in ice-cold 4% paraformaldehyde for 30 min and then washed twice in PBS. Samples were stained with Alexa Fluor 546-phalloidin (20 nmol/L) for 1 h. Nuclei were stained with DAPI (1  $\mu$ g/mL) for 10 min at room temperature. Cells were stained with 50  $\mu$ g/mL fluorescent phalloidin-conjugate in PBS for 20 min at room temperature and then washed three times with PBS to remove unbound phalloidin-conjugate. Images were acquired under a laser scanning confocal microscope (TCS SP2, Leica, Germany). Image J software was used to quantify and compare cell morphology on PLLA nanofibers and flat polymer films. There were 50 cells analyzed for the cell shape measurements in each group.

**Alkaline Phosphatase Activity Assay.** Alkaline phosphatase activity measurement was performed using an alkaline phosphatase assay kit (Abcam). Three replicates were performed for all groups, and each replicate was prepared by pooling culture supernatants from three wells. Culture supernatants (30  $\mu$ L) were combined with alkaline buffer and 50  $\mu$ L of *p*-nitrophenyl phosphate and then incubated for 60 min. The reaction was stopped with 20  $\mu$ L of stop solution (provided in the kit). The absorbance was then measured at 405 nm. ALP activity was calculated with the following formula: ALP activity (U/mL) = amount of pNP generated/volume of sample/reaction time.

**RT-qPCR Analysis.** hBMSCs cultured on PLLA nanofibers and flat polymer films with or without OS were harvested at 4, 7, 14, and 21 days and quantitatively assessed using an RT-PCR system. Total RNA was extracted using an RNeasy mini kit (QIAGEN) as per the manufacturer's instructions. RNA (1  $\mu$ g) was added to a 20  $\mu$ L reverse transcription reaction mixture containing  $10\times$  reverse transcription buffer, 25 mM MgCl<sub>2</sub>,

TABLE 2. Primers for Real-Time PCR

gene	forward primers (5'→3')	reverse primers (5'→3')
BMP2	GGTATCACGCCTTTACTGCC	ACACCCACACCCCTCCACAA
RUNX2	CCGCACGACAACCGCACCAT	CGCTCCGCCACAAATCTC
SPP1	GTGTGGTTATGGACTGAGG	CTCGCTTCCAGTGTGAGG
COL1A1	AGAACATCACTACCACTGC	ATGTCCAAAGGTGCAATATC
SPARC	CAAATACATCCCCCTTGCC	GATCTTCTTCACCCGAGCTT
BSP	CTGGCACAGGTATACAGGGTTAG	ACTGGTGCCGTTTATGCCTTG
GAPDH	AGAAGGCTGGGGCTCATTG	AGGGGCCATCCACAGCTTC

10 mM dNTPs, recombinant RNasin ribonuclease inhibitor, 15 U AMV reverse transcriptase, and 0.5  $\mu$ g of oligo (dT) primer. RT-qPCR was performed according to the method described by the manufacturer: 45 cycles of 95 °C for 30 s, 60 °C for 30 s, and 72 °C for 30 s. Glyceraldehyde-3-phosphate dehydrogenase (GAPDH) was used as the housekeeping gene. Quantification of gene expression was based on the CT value for each sample, which was calculated as the average of three replicate measurements, and each replicate was prepared by pooling cell lysates from three wells. The primers were designed based on the sequences of the corresponding human mRNA in GenBank (Table 2).

**Microarray Analysis.** Total RNA from hBMSCs after 4, 7, 14, and 21 days of culture on PLLA nanofibers and flat polymer films with or without OS was extracted using the RNeasy mini kit. Total RNA samples were analyzed by CapitalBio (CapitalBio Corp, Beijing, China). The quality and quantity of each RNA sample were confirmed using an ultraviolet spectrophotometer (NanoDrop, ND-1000) and 1.2% formaldehyde agarose gel electrophoresis. Briefly, 200 ng of total RNA was used to synthesize first-strand cDNA followed by double-stranded cDNA using a Message Amp Premier RNA amplification kit and PCR apparatus (MJ, PTC-225). Biotin-labeled cRNA was synthesized using a MessageAmp Premier RNA amplification kit (Ambion). The concentration of cRNA was measured using the NanoDrop ND-1000, and 15  $\mu$ g of fragmented cRNA was hybridized to each GeneChip Human Genome U133 Plus 2.0 Array (Affymetrix), which contains more than 54 000 probe sets to cover over 47 000 transcripts and variants, at 45 °C for 16 h (Affymetrix Hybridization Oven 640) according to the manufacturer's instructions. After hybridization, the arrays were washed, stained with streptavidin phycoerythrinonan using an Affymetrix Fluidics Station 450, and followed by scanning with the Affymetrix Scanner 3000 7G. Three replicates of the microarray experiment were performed until high reproducibility was achieved. Each replicate was made by pooling cell lysates from three wells.

**Data Processing.** Data preprocessing and normalization were performed using the Bioconductor Affymetrix package.<sup>48</sup> For the analysis, two factors were used: topography (control, random, aligned, and OS groups) and time (4, 7, 14, and 21 days). To select the differentially expressed genes, threshold values of  $\geq 1.5$  or  $\leq 0.667$  of ratio change were used. The hierarchical clustering was performed on log2 transformed data using Cluster 3.0 software; then the clustering results were visualized by the Treeview program. Then in comparative analysis, we applied a two class unpaired method in the Significant Analysis of Microarray software (SAM, version 3.02) to identify significantly differentially expressed genes between TEST and CONTROL groups.

**Gene Ontology.** The expression of genes significantly altered in the four groups was categorized by gene ontology using Molecule Annotation System V3.0 (CapitalBio). Altered gene expression was compared with the expression of all genes present on the array, and over-represented ontologies were identified automatically by the software with  $p < 0.05$  considered significant.

**Pathway Analysis.** We assessed pathways with the greatest representation of gene expression that was significantly altered by topography based on KEGG pathway annotations. Over-representation of genes in a KEGG pathway is present if a larger fraction of genes within that pathway is expressed differentially.

**Statistical Analysis.** The experimental results and measurements were performed in triplicate and expressed as the mean  $\pm$  standard deviation (SD). Statistical analysis was performed using the Student's paired *t*-test, and  $p < 0.05$  was considered significant.

**Conflict of Interest:** The authors declare no competing financial interest.

**Acknowledgment.** The authors acknowledge the National Basic Research Program of China (2012CB933900), the National Natural Science Foundation of China (81171000), the National High Technology Research and Development Program of China (2012AA022501), and the support of Peking University-Tsinghua University Joint Center for Life Sciences.

**Supporting Information Available:** Illustrations of the focal adhesion, MAPK, TGF- $\beta$ , and Wnt signaling pathways derived from the KEGG database with genes were mapped according to their expression influenced by random nanofibers. This material is available free of charge via the Internet at <http://pubs.acs.org>.

## REFERENCES AND NOTES

- Mackay, A. M.; Beck, S. C.; Murphy, J. M.; Barry, F. P.; Chichester, C. O.; Pittenger, M. F. Chondrogenic Differentiation of Cultured Human Mesenchymal Stem Cells from Marrow. *Tissue Eng.* **1998**, *4*, 415–428.
- Engler, A. J.; Sen, S.; Sweeney, H. L.; Discher, D. E. Matrix Elasticity Directs Stem Cell Lineage Specification. *Cell* **2006**, *126*, 677–689.
- Nesti, L. J.; Jackson, W. M.; Shanti, R. M.; Koehler, S. M.; Aragon, A. B.; Bailey, J. R.; Sracic, M. K.; Freedman, B. A.; Giuliani, J. R.; Tuan, R. S. Differentiation Potential of Multipotent Progenitor Cells Derived from War-Traumatized Muscle Tissue. *J. Bone Jt. Surg., Am. Vol.* **2008**, *90*, 2390–2398.
- Carlson, A. L.; Florek, C. A.; Kim, J. J.; Neubauer, T.; Moore, J. C.; Cohen, R. I.; Kohn, J.; Grumet, M.; Moghe, P. V. Microfibrous Substrate Geometry as a Critical Trigger for Organization, Self-Renewal, and Differentiation of Human Embryonic Stem Cells within Synthetic 3-Dimensional Microenvironments. *FASEB J.* **2012**, *26*, 3240–3251.
- Wilson, A.; Trumpp, A. Bone-Marrow Haematopoietic-Stem-Cell Niches. *Nat. Rev. Immunol.* **2006**, *6*, 93–106.
- Mitsiadis, T. A.; Barrandon, O.; Rochat, A.; Barrandon, Y.; De Bari, C. Stem Cell Niches in Mammals. *Exp. Cell Res.* **2007**, *313*, 3377–3385.
- Dalby, M. J.; McCloy, D.; Robertson, M.; Wilkinson, C. D.; Oreffo, R. O. Osteoprogenitor Response to Defined Topographies with Nanoscale Depths. *Biomaterials* **2006**, *27*, 1306–1315.
- Dalby, M. J.; Hart, A.; Yarwood, S. J. The Effect of the RACK1 Signalling Protein on the Regulation of Cell Adhesion and Cell Contact Guidance on Nanometric Grooves. *Biomaterials* **2008**, *29*, 282–289.
- Dalby, M. J.; McCloy, D.; Robertson, M.; Agheli, H.; Sutherland, D.; Affrossman, S.; Oreffo, R. O. Osteoprogenitor Response to Semi-Ordered and Random Nanotopographies. *Biomaterials* **2006**, *27*, 2980–2987.
- Ravichandran, R.; Liao, S.; Ng, C.; Chan, C. K.; Raghunath, M.; Ramakrishna, S. Effects of Nanotopography on Stem Cell Phenotypes. *World J. Stem Cells* **2009**, *1*, 55–66.

11. Kaur, G.; Valarmathi, M. T.; Potts, J. D.; Jabbari, E.; Sabo-Attwood, T.; Wang, Q. Regulation of Osteogenic Differentiation of Rat Bone Marrow Stromal Cells on 2D Nanorod Substrates. *Biomaterials* **2010**, *31*, 1732–1741.
12. Zhu, H.; Cao, B.; Zhen, Z.; Laxmi, A. A.; Li, D.; Liu, S.; Mao, C. Controlled Growth and Differentiation of MSCs on Grooved Films Assembled from Monodisperse Biological Nanofibers with Genetically Tunable Surface Chemistries. *Biomaterials* **2011**, *32*, 4744–4752.
13. Kim, H. W.; Lee, H. H.; Knowles, J. C. Electrospinning Biomedical Nanocomposite Fibers of Hydroxyapatite/Poly(lactic acid) for Bone Regeneration. *J. Biomed. Mater. Res., Part A* **2006**, *79*, 643–649.
14. Hu, J.; Liu, X.; Ma, P. X. Induction of Osteoblast Differentiation Phenotype on Poly(L-lactic acid) Nanofibrous Matrix. *Biomaterials* **2008**, *29*, 3815–3821.
15. Yin, Z.; Chen, X.; Chen, J. L.; Shen, W. L.; Hieu Nguyen, T. M.; Gao, L.; Ouyang, H. W. The Regulation of Tendon Stem Cell Differentiation by the Alignment of Nanofibers. *Biomaterials* **2010**, *31*, 2163–2175.
16. Wang, B.; Cai, Q.; Zhang, S.; Yang, X.; Deng, X. The Effect of Poly (L-lactic acid) Nanofiber Orientation on Osteogenic Responses of Human Osteoblast-Like MG63 Cells. *J. Mech. Behav. Biomed. Mater.* **2011**, *4*, 600–609.
17. Wang, Y.; Gao, R.; Wang, P. P.; Jian, J.; Jiang, X. L.; Yan, C.; Lin, X.; Wu, L.; Chen, G. Q.; Wu, Q. The Differential Effects of Aligned Electrospun PHBHHx Fibers on Adipogenic and Osteogenic Potential of MSCs through the Regulation of PPARgamma Signaling. *Biomaterials* **2012**, *33*, 485–493.
18. Lim, S. H.; Liu, X. Y.; Song, H.; Yarema, K. J.; Mao, H. Q. The Effect of Nanofiber-Guided Cell Alignment on the Preferential Differentiation of Neural Stem Cells. *Biomaterials* **2010**, *31*, 9031–9039.
19. Karuri, N. W.; Liliensiek, S.; Teixeira, A. I.; Abrams, G.; Campbell, S.; Nealey, P. F.; Murphy, C. J. Biological Length Scale Topography Enhances Cell-Substratum Adhesion of Human Corneal Epithelial Cells. *J. Cell Sci.* **2004**, *117*, 3153–3164.
20. Oh, S.; Brammer, K. S.; Li, Y. S.; Teng, D.; Engler, A. J.; Chien, S.; Jin, S. Stem Cell Fate Dictated Solely by Altered Nanotube Dimension. *Proc. Natl. Acad. Sci. U.S.A.* **2009**, *106*, 2130–2135.
21. Datta, N.; Pham, Q. P.; Sharma, U.; Sikavitsas, V. I.; Jansen, J. A.; Mikos, A. G. *In Vitro* Generated Extracellular Matrix and Fluid Shear Stress Synergistically Enhance 3D Osteoblastic Differentiation. *Proc. Natl. Acad. Sci. U.S.A.* **2006**, *103*, 2488–2493.
22. Ruckh, T. T.; Kumar, K.; Kipper, M. J.; Papat, K. C. Osteogenic Differentiation of Bone Marrow Stromal Cells on Poly-(Epsilon-Caprolactone) Nanofiber Scaffolds. *Acta Biomater.* **2010**, *6*, 2949–2959.
23. Pashuck, E. T.; Stevens, M. M. Designing Regenerative Biomaterial Therapies for the Clinic. *Sci. Transl. Med.* **2012**, *4*, 160sr4.
24. Weiner, S.; Traub, W.; Wagner, H. D. Lamellar Bone: Structure-Function Relations. *J. Struct. Biol.* **1999**, *126*, 241–255.
25. Elsdale, T.; Bard, J. Collagen Substrata for Studies on Cell Behavior. *J. Cell Biol.* **1972**, *54*, 626–37.
26. Holzwarth, J. M.; Ma, P. X. Biomimetic Nanofibrous Scaffolds for Bone Tissue Engineering. *Biomaterials* **2011**, *32*, 9622–9629.
27. Mathur, A.; Moore, S. W.; Sheetz, M. P.; Hone, J. The Role of Feature Curvature in Contact Guidance. *Acta Biomater.* **2012**, *8*, 2595–2601.
28. Laco, F.; Grant, M. H.; Black, R. A. Collagen-Nanofiber Hydrogel Composites Promote Contact Guidance of Human Lymphatic Microvascular Endothelial Cells and Directed Capillary Tube Formation. *J. Biomed. Mater. Res., Part A* **2013**, *101A*, 1787–1799.
29. Pan, Z.; Yan, C.; Peng, R.; Zhao, Y.; He, Y.; Ding, J. Control of Cell Nucleus Shapes via Micropillar Patterns. *Biomaterials* **2012**, *33*, 1730–1735.
30. Kumar, G.; Tison, C. K.; Chatterjee, K.; Pine, P. S.; McDaniel, J. H.; Salit, M. L.; Young, M. F.; Simon, C. G., Jr. The Determination of Stem Cell Fate by 3D Scaffold Structures through the Control of Cell Shape. *Biomaterials* **2011**, *32*, 9188–9196.
31. Andersson, A. S.; Backhed, F.; von Euler, A.; Richter-Dahlfors, A.; Sutherland, D.; Kasemo, B. Nanoscale Features Influence Epithelial Cell Morphology and Cytokine Production. *Biomaterials* **2003**, *24*, 3427–3436.
32. Fu, J.; Wang, Y. K.; Yang, M. T.; Desai, R. A.; Yu, X.; Liu, Z.; Chen, C. S. Mechanical Regulation of Cell Function with Geometrically Modulated Elastomeric Substrates. *Nat. Methods* **2010**, *7*, 733–736.
33. Gardel, M. L.; Schneider, I. C.; Aratyn-Schaus, Y.; Waterman, C. M. Mechanical Integration of Actin and Adhesion Dynamics in Cell Migration. *Annu. Rev. Cell Dev. Biol.* **2010**, *26*, 315–333.
34. Seidlits, S. K.; Khaing, Z. Z.; Petersen, R. R.; Nickels, J. D.; Vanscoy, J. E.; Shear, J. B.; Schmidt, C. E. The Effects of Hyaluronic Acid Hydrogels with Tunable Mechanical Properties on Neural Progenitor Cell Differentiation. *Biomaterials* **2010**, *31*, 3930–3940.
35. Baker, S. C.; Rohman, G.; Southgate, J.; Cameron, N. R. The Relationship between the Mechanical Properties and Cell Behaviour on PLGA and PCL Scaffolds for Bladder Tissue Engineering. *Biomaterials* **2009**, *30*, 1321–1328.
36. Schwarz, U. S.; Gardel, M. L. United We Stand: Integrating the Actin Cytoskeleton and Cell-Matrix Adhesions in Cellular Mechanotransduction. *J. Cell Sci.* **2012**, *125*, 3051–3060.
37. Bar-Nur, O.; Russ, H. A.; Efrat, S.; Benvenisty, N. Epigenetic Memory and Preferential Lineage-Specific Differentiation in Induced Pluripotent Stem Cells Derived from Human Pancreatic Islet Beta Cells. *Cell Stem Cell* **2011**, *9*, 17–23.
38. Xu, Y.; Wagner, D. R.; Bekerman, E.; Chiou, M.; James, A. W.; Carter, D.; Longaker, M. T. Connective Tissue Growth Factor in Regulation of RhoA Mediated Cytoskeletal Tension Associated Osteogenesis of Mouse Adipose-Derived Stromal Cells. *PLoS One* **2010**, *5*, e11279.
39. Tseng, P. C.; Young, T. H.; Wang, T. M.; Peng, H. W.; Hou, S. M.; Yen, M. L. Spontaneous Osteogenesis of MSCs Cultured on 3D Microcarriers through Alteration of Cytoskeletal Tension. *Biomaterials* **2012**, *33*, 556–564.
40. Kilian, K. A.; Bugarija, B.; Lahn, B. T.; Mrksich, M. Geometric Cues for Directing the Differentiation of Mesenchymal Stem Cells. *Proc. Natl. Acad. Sci. U.S.A.* **2010**, *107*, 4872–4877.
41. Tsimbouri, P. M.; Murawski, K.; Hamilton, G.; Herzyk, P.; Oreffo, R. O.; Gadegaard, N.; Dalby, M. J. A Genomics Approach in Determining Nanotopographical Effects on MSC Phenotype. *Biomaterials* **2013**, *34*, 2177–2184.
42. McMurray, R. J.; Gadegaard, N.; Tsimbouri, P. M.; Burgess, K. V.; McNamara, L. E.; Tare, R.; Murawski, K.; Kingham, E.; Oreffo, R. O.; Dalby, M. J. Nanoscale Surfaces for the Long-Term Maintenance of Mesenchymal Stem Cell Phenotype and Multipotency. *Nat. Mater.* **2011**, *10*, 637–644.
43. Kaur, G.; Valarmathi, M. T.; Potts, J. D.; Jabbari, E.; Sabo-Attwood, T.; Wang, Q. Regulation of Osteogenic Differentiation of Rat Bone Marrow Stromal Cells on 2D Nanorod Substrates. *Biomaterials* **2010**, *31*, 1732–1741.
44. Ruckh, T. T.; Kumar, K.; Kipper, M. J.; Papat, K. C. Osteogenic Differentiation of Bone Marrow Stromal Cells on Poly-(Epsilon-Caprolactone) Nanofiber Scaffolds. *Acta Biomater.* **2010**, *6*, 2949–2959.
45. Castillo, A. B.; Blundo, J. T.; Chen, J. C.; Lee, K. L.; Yereddi, N. R.; Jang, E.; Kumar, S.; Tang, W. J.; Zarrin, S.; Kim, J. B.; Jacobs, C. R. Focal Adhesion Kinase Plays a Role in Osteoblast Mechanotransduction *in Vitro* but Does Not Affect Load-Induced Bone Formation *in Vivo*. *PLoS One* **2012**, *7*, e43291.
46. Goldmann, W. H. Mechanotransduction and Focal Adhesions. *Cell Biol. Int.* **2012**, *36*, 649–652.

47. Chowdhury, S. R.; Ng, M. H.; Hassan, N. S.; Aminuddin, B. S.; Ruszymah, B. H. Identification of Suitable Culture Condition for Expansion and Osteogenic Differentiation of Human Bone Marrow Stem Cells. *Hum. Cell* **2012**, *25*, 69–77.
48. Tusher, V. G.; Tibshirani, R.; Chu, G. Significance Analysis of Microarrays Applied to the Ionizing Radiation Response. *Proc. Natl. Acad. Sci. U.S.A.* **2001**, *98*, 5116–5121.